Gómez-de la Cruz, F. J., Palomar-Torres, A., Pérez-Latorre, F. J., & Cruz-Peragón, F. (2023). Convective drying of mango stone for use as biomass. Environmental Research, 227, 115742.

https://doi.org/10.1016/j.envres.2023.115742

Convective drying of mango stone for use as biomass.

Authors.

Francisco J. Gómez-de la Cruz[1*], Amalia Palomar-Torres[1], Francisco J. Pérez-Latorre[1], Fernando Cruz-Peragón[1].

[1]Dep. of Mechanical and Mining Engineering, Escuela Politécnica Superior de Jaén, University of Jaén, Campus Las Lagunillas s/n, 23071, Jaén (Spain).

Abstract.

Mango stone is an interesting biomass by-product with a considerable net calorific value. Mango production has significantly risen in the last few years, meaning that mango waste has increased as well. However, mango stone has a moisture content of about 60% (wet basis) and it is very important to dry the samples for using them in electrical and thermal energy production. In this paper, the main parameters involved in the mass transfer during drying are determined. Drying was carried out in a convective dryer through a set of experiments based on five drying air temperatures (100ºC, 125ºC, 150ºC, 175ºC and 200ºC) and three air velocities (1 m/s, 2 m/s and 3 m/s). Drying times ranged between 2 and 23 hours. The drying rate was calculated from the Gaussian model whose values ranged from $1.5 \cdot 10^{-6}$ to $6.3 \cdot 10^{-4}$ s^{-1}. Effective diffusivity was obtained as an overall parameter in the mass diffusion for each test. These values were found between $0.71 \cdot 10^{-9}$ and $13.6 \cdot 10^{-9}$ m^2/s. The activation energy was calculated from

*Corresponding author: Tel.: +34 953213002; Fax: +34 953212870; E-mail address: fjgomez@ujaen.es

the Arrhenius law for each test, made at different air velocities. These values were 36.7, 32.2 and 32.1 kJ/mol for 1, 2 and 3 m/s, respectively. This study provides information for future works on design, optimization and numerical simulation models in convective dryers for standard mango stone pieces according to industrial drying conditions.

Keywords: Mango stone; Biomass; Waste recovery; Mass transfer; Drying rate; Effective diffusivity.

Nomenclature

a, b, c, d, e, f	Coefficients of the Two-term mathematical model
D_{eff}	Effective moisture diffusivity (m^2/s)
D_0	Pre-exponential factor of the Arrhenius equation (m^2/s)
E_a	Activation energy (kJ/mol)
L	Half-thickness of the slab (m)
m	Mass (kg)
N	Number of data
R	Universal gas constant ($kJ \cdot mol^{-1} \cdot K^{-1}$)
R^2	Coefficient of determination
$RMSE$	Root mean square error
s	Straight line's slope
t	Time (s)
T	Temperature (ºC, K)
v	Velocity ($m \cdot s^{-1}$)
x	Spatial dimension (m)

X	Moisture content (kg moisture/kg dry matter)
XR	Dimensionless moisture ratio
x_v	Drying rate (s^{-1})

Subindex

cal	calculated
ds	dry solid
e	equilibrium
exp	experimental
t	at time t
w	water
0	initial

1. Introduction.

The mango fruit (*Mangifera indica L.*) belongs to the Anacardiaceae family. It is a sweet fruit with great benefits to human health (Torres-León et al., 2016). Its cultivation has expanded all over the world, mainly in coastal areas and subtropical climate zones. There are about 350 varieties of mango in the world, which are cultivated in over 100 countries. Mango is mainly consumed as fresh fruit, although it is used for juice, nectar, preserves, puree, dried fruit, jams, ice creams, etc. (Maneepun and Yunchalad, 2004). The world's production exceeded 55 million tonnes in 2019 (Manhongo et al., 2021). India is the world's top producer whose production for that year was 21,800,000 tonnes, which is the equivalent of 40% of total output. Countries such as China, Thailand,

74 Indonesia, Pakistan and Mexico had a production of 4,800,000 tonnes, 3,790,000
75 tonnes, 3,000,000 tonnes, 2,300,000 tonnes and 2,100,000 tonnes, respectively
76 (FAOSTAT, 2018).

77 The food industry produces large quantities of by-products and wastes. Because
78 of that, there is a global concern regarding their use and their recycling. In general,
79 industries based on the production of juices and pulp fruits generate the vast majority of
80 waste because of the removal of skin, pits and seeds (da Silva and Jorge, 2014). Wastes
81 present serious management problems, from both the economic and environmental
82 points of view. However, food industry wastes can be reused in other production
83 systems, foremost in thermal and electrical energy production (Mirabella et al., 2014;
84 Ishaq and Dincer, 2020).

85 Up until now, the mango processing industry does not provide efficient, profitable
86 and viable systems for wastes disposal, which means a new source of environmental
87 pollution (Ajila et al., 2007). Depending on the variety, mango stone represents between
88 10% and 25% of the fruit's total weight (Torres-León et al., 2016). After one year, the
89 mango fruit generates between five and thirteen million tonnes of mango stone, and
90 these wastes, nowadays, are not used for commercial and energetic purposes
91 (Leanpolchareanchai et al., 2014). In this sense, mango stone can be classified as a
92 biomass by-product for thermal and electrical energy generation (Perea-Moreno, A. et
93 al., 2018). Due to its high moisture content, drying is essential for improving the
94 combustion yield and for avoiding water vapour condensation, which presents adverse
95 effects in boilers (Saidur et al., 2011). Furthermore, drying improves the storage and
96 transport conditions (Gómez-de la Cruz, F. J. et al., 2017).

97 Nevertheless, drying is a thermal process linked to high-energy consumption. For
98 this reason, to optimize the process it is vital to know the main parameters involved

during the drying of mango (Chupawa et al., 2022; Perazzini et al., 2021). All these parameters are very important in mass transfer phenomena. These parameters, obtained in experimental equipment, provide information to improve the design of industrial dryers, and optimization of the drying conditions such as temperature, velocities and sample size. Furthermore, these variables can be used in numeric simulation in Computational Fluid Dynamics to validate the drying models (Kaya et al., 2008; Ture and Chandramohan, 2021; Jha and Tripathy, 2021).

The drying of mango fruit has been widely studied in the literature for nutritional purposes. However, the drying of mango wastes for efficient biomass production, mainly mango stone, has been addressed in a few works. (Perea-Moreno, A. et al., 2018) carried out both an ultimate analysis and a proximate analysis. Moreover, they determined the higher and lower heating values of mango stone. In this research, the mango stone moisture content was 59.7% (wet basis). On the other hand, (Wilkins et al., 2018) studied the drying of mango stone placed on trays in a solar dryer under uncontrolled environments. They obtained drying rate models for these drying conditions.

Industrial convective dryers are the best equipment to dry wet products obtaining high drying rates, drying times very short with respect to others such as: microwave drying, infrared dryers, solar dryers and fluidized bed dryers (Gómez-de la Cruz, F. J et al., 2015b). Furthermore, except solar dryers, convective dryers present low energy consumption for the same drying conditions. In this sense, this work presents detailed research on the drying of mango stone (per unit) in an experimental convective dryer through a set of experiments using three drying air velocities and five drying air temperatures, fifteen experiments in total. Drying times and drying rates experimental data are fitted with Gaussian models. Effective diffusivity values are obtained thanks to

124 the solution for the plane sheet of the partial differential equation of mass diffusion.
125 Finally, activation energy values are determined from an Arrhenius law. The results
126 obtained will contribute to defining the optimal drying conditions (temperature and
127 velocity of the drying air) to reduce the drying times, and increase the drying rate and
128 energy efficiency of the mango stone pieces avoiding the risk of combustion. The main
129 findings are commented and possible future works are exposed in the conclusions.
130
131 **2. Materials and methods.**
132
133 2.1. Raw Material.
134
135 Mango fruits were acquired in a supermarket in the southern region of Spain (on the
136 Andalusian coast). After purchasing them, the samples were frozen until use. The
137 studies were carried out using the Kent variety with a weight between 500 and 600
138 grams. The mango stone samples presented a weight between 55 and 65 grams,
139 approximately 10% of the total weight of the fruit. The samples were measured to
140 obtain the following dimensions: 96.7 ± 0.3 mm (length), 52.1 ± 0.1 mm (width) and
141 19.16 ± 0.7 mm (thickness). To know the initial moisture content, the samples were
142 dried in an oven (Memmert GmbH + Co.KG, SNB 167 Model 100, Germany) at 105 ºC
143 for 24 hours. The drying process has been made on five different samples. An average
144 moisture content of 58.5 ± 2.3% (wet basis) was found. The same procedure was
145 applied to obtain the equilibrium moisture content which was estimated at 5.3 ± 1.1%
146 (wet basis). Environmental conditions of the laboratory during the experiments were
147 25ºC and 40% of room temperature and air relative humidity, respectively.

148 Furthermore, a proximate and elemental analysis was carried out from dried
149 samples. The ultimate analysis was performed using a LECO TruSpect CHN2 elemental
150 analyzer according to ASTM D5373. On the other hand, to carry out the proximate
151 analysis a Thermogravimetric Analyzer TGA (Mettler Toledo) was used based on
152 ASTM E790/830/897 standard. The higher heating value (HHV) and net calorific value
153 (NVC) of this waste were determined using the PARR 6050 bomb calorimeter
154 according to ASTM D240 standard. These experiments were made in triplicate. Table 1
155 shows the results obtained.
156
157 **Table 1.** Elemental analysis, proximate analysis and higher heating value (HHV) and net calorific
158 value (NCV) of mango stone.

Analysis	Element	Value	
		Seed	Shell
Elemental analysis (%)	C	43.36 ± 1.26	43.32 ± 1.16
	H	5.73 ± 0.18	5.42 ± 015
	N	1.12 ± 0.05	0.39 ± 0.03
	S	0.17 ± 0.01	0.32 ± 0.03
	O (by difference)	49.62 ± 1.28	50.55 ± 1.42
Proximate analysis (%)	Moisture	4.70 ± 0.08	4.74 ± 0.90
	Ash	2.57 ± 0.84	1.92 ± 0.75
	Volatile Matter	73.92 ± 3.34	75.5 ± 1.08
	Fixed Carbon (by difference)	18.77 ± 2.50	17.69 ± 1.30
Higher Heating Value (HHV) (MJ/kg)		19.70 ± 0.22	20.21 ± 0.25
Net Calorfic Value (NCV) (MJ/kg)		18.41 ± 0.18	18.99 ± 0.17

159
160
161 2.2. Design of experiments and procedures in the drying equipment.
162
163 To perform the drying experiments, a set of experiments based on two variables, air
164 temperature and air velocity, has been proposed. The tests were performed at five air
165 temperatures and three air velocities. The range of drying air temperatures was proposed
166 between 100 ºC and 200 ºC, and for the drying air velocities between 1 m/s and 3 m/s.

This is the range of values in which the drying of biomass is carried out in industrial convective dryers. For temperatures and velocities higher than 200 ºC and 3 m/s volatile matter and risk of fire can occur (Gómez-de la Cruz, F. J. et al., 2014; Arjona et al., 1999). Considering the natural inhomogeneity of the by-products, all experiments were performed in triplicate, with forty-five isothermal experiments in total. Table 2 details each of the drying experiments for the mango stone samples.

Table 2. Design of experiments for drying of mango stone.

TEST	Temperature (°C)	Velocity (m/s)
A	100 ± 1	
B	125 ± 1	
C	150 ± 1	1 ± 0.1
D	175 ± 1	
E	200 ± 1	
F	100 ± 1	
G	125 ± 1	
H	150 ± 1	2 ± 0.1
I	175 ± 1	
J	200 ± 1	
K	100 ± 1	
L	125 ± 1	
M	150 ± 1	3 ± 0.1
N	175 ± 1	
O	200 ± 1	

The experiments were performed in a convective dryer designed by the members of the INGEMER-TEP250 research group of the University of Jaén. The drying equipment has already been described in other research (Gómez-de la Cruz, F. J., Palomar-Carnicero, Hernández-Escobedo and Cruz-Peragón, 2021) (figure 1). In summary, the equipment is formed by a blower, a group of electrical resistances (45 kW in total) and a tunnel of square section (0.15 m x 0.15 m x 2 m). A Variable Frequency Drive (VFD) connected to an electric AC motor allows for programming the air velocity. The resistances group heats the air to the test temperature. A PT100 sensor measures the

drying temperature before the samples. This sensor is connected to a PID control, which regulates the drying air temperature with a tolerance of ± 1ºC. The mango stone samples are placed on a basket, which is linked to a precision balance (Blauscal AH1200) with an error of ± 0.01 g. The balance is connected to a personal computer by a USB port, which measures the variation of mass by software developed by the authors. The information is stored in files, which are treated with the MATLAB® program.

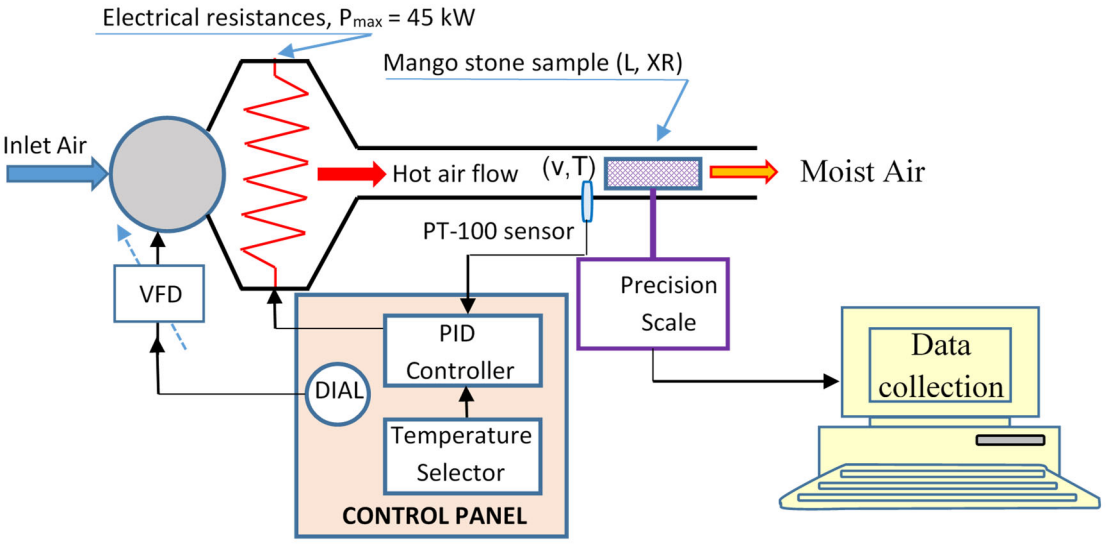

Figure 1: Scheme of the experimental convective dryer.

2.3. Drying curves and drying rates.

Moisture content represents the water contained in the solid. Moisture content can be measured on a wet basis or a dry basis. In general, drying curves represent the variation of moisture ratio, which is based on the moisture content on a dry basis, about time (Eq (1)).

$$X = \frac{m_w}{m_{ds}} = \frac{m_t(t) - m_{ds}}{m_{ds}} \quad (1)$$

where m_w is the mass of water, $m_t(t)$ is the total mass at time t and m_{ds} is the dry mass of the sample. The moisture ratio can be expressed as follows:

$$XR = \frac{X_t - X_e}{X_0 - X_e} \quad (2)$$

where X_t is the moisture content at time t, X_0 is the initial moisture content and X_e is the equilibrium moisture content. For low moisture content, the equilibrium moisture content value can be neglected and, therefore, the dimensionless moisture ratio can be expressed as:

$$XR = \frac{X_t}{X_0} \quad (3)$$

Due to the complexity of studying the drying process, drying curves are fitted with empirical, semi-empirical or semi-theoretical mathematical functions. One of the best models that fit the drying curve's experimental data is the Gaussian model (Gómez-de la Cruz, F. J. et al., 2014). The Two-term Gaussian model allows fitting the drying curves with a coefficient of determination values of one (Eq (4)).

$$XR = a \cdot \exp\left[-\left(\frac{t-b}{c}\right)^2\right] + d \cdot \exp\left[-\left(\frac{t-e}{f}\right)^2\right] \quad (4)$$

In this model, t is the independent variable (s) and a, b, c, d, e and f are constants.

Although the model has six constants, presents great advantages over other models. A good fit in the drying curves removes the errors made when the derivate function is calculated to approximate the drying rate curves (Gómez-de la Cruz, F. J., Palomar-Carnicero, Hernández-Escobedo and Cruz-Peragón, 2020). Analytically and experimentally, the drying rates can be expressed as follows:

$$x_v = -\frac{d(XR)}{dt} \approx -\frac{XR_{t+\Delta t} - XR_t}{\Delta t} \quad (5)$$

where $XR_{t+\Delta t}$ and XR_t indicate the moisture content at time $t + \Delta t$ and the moisture content at time t, respectively, and t is the drying time (s). Subsequently, drying rate can be expressed as a function whose independent variables are the drying air temperature and moisture ratio for each air velocity, $x_v = f(XR, T)$.

2.4. Effective diffusivity and Arrhenius equation.

Diffusion phenomenon within the solid is based on simultaneous coupled heat and mass transfer that includes several manifestations in the water elimination process such as:

-Transport mechanisms like diffusion by capillary movements, osmosis and thermally driven for liquid state and Knudsen diffusion and Soret effect in the vapour state.

-Volumetric sources, mainly phase change (evaporation and desorption)

-Drying forces, among which are surface tension and gas-liquid pressure.

On the other hand, at high temperatures not only appear convection and conduction

phenomena, but also radiation. In this sense, the effective diffusivity (D_{eff}) of mango stone can be obtained as a parameter that involves all these phenomena from the solution of the partial differential equation of mass diffusion for the plane sheet condition.

$$\frac{\partial(XR)}{\partial t} = D_{eff}\frac{\partial^2(XR)}{\partial x^2} \quad (6)$$

Eq. (6) is called the Fick'second law of diffusion, and on this occasion has been proposed in Cartesian coordinates for one sole dimension, x axis (m). The solution for a non-steady state, plane sheet and uniform initial distribution considering surface concentration equal was obtained by (Crank, 1975):

$$XR = \sum_{n=0}^{\infty}\frac{8}{(2n+1)^2\,\pi^2}\exp\left(-\frac{(2n+1)^2\,\pi^2 D_{eff}\,t}{4L^2}\right) \quad (7)$$

where L represents the half-thickness of the slab (m). The solution can be simplified to the first term for long drying times with good results in the solution as follows (Chen, C. et al., 2020):

$$XR = \frac{8}{\pi^2}\exp\left(-\frac{\pi^2 D_{eff}\,t}{4L^2}\right) \quad (8)$$

This last equation makes it possible to obtain the effective diffusivity by plotting experimental drying data in terms of $ln\ XR$ versus drying time for each experiment. The slope of these curves is used to calculate this variable as follows:

$$D_{eff} = -s\frac{4L^2}{\pi^2} \quad (9)$$

where s is the straight line's slope that fits the curves $ln\ XR - t$. In this case, the effective diffusivity value is obtained as a constant value during all drying experiments.

On the other hand, effective diffusivity depends on the temperature and can be calculated from an Arrhenius-type equation as follows:

$$D_{eff} = D_0 exp\left(-\frac{E_a}{RT}\right) \quad (10)$$

where D_0 is the pre-exponential factor (m^2/s), R is the universal gas constant ($kJ \cdot mol^{-1} \cdot K^{-1}$), T is the absolute temperature (K) and E_a is the activation energy ($kJ \cdot mol^{-1}$). Applying logarithm in both side of the equation, activation energy and pre-exponential factor values can be obtained from the slope and interception of the plot $ln\ D_{eff} - 1/T$ (Eq. 11).

$$\ln D_{eff} = \ln D_0 - \frac{E_a}{R}\frac{1}{T} \quad (11)$$

Activation energy represents the minimum energy to begin the diffusion phenomenon within of the sample.

2.5. Statistical parameters to evaluate the mathematical models.

To verify the quality of the fit in the mathematical models, we have used statistical parameters such as the coefficient of determination and the root mean square

297 error. These equations are:

298

299 $$R^2 = \sum_{i=1}^{N} \frac{\left(XR_{cal,i} - XR_{exp,i}\right)^2}{\left(XR_{exp,i} - \overline{XR_{exp,i}}\right)^2} \quad (12)$$

300

301 $$RMSE = \sqrt{\frac{1}{N}\sum_{i=1}^{N}\left(XR_{exp,i} - XR_{cal,i}\right)^2} \quad (13)$$

302

303 where N is the number of data and the subscripts exp and cal mean experimental and

304 calculated, respectively.

305

306 **3. Results and discussion.**

307

308 3.1. Drying curves and drying times analysis.

309

310 A moisture ratio in the function of drying time is represented for each drying air

311 velocity in figure 2a-c. Each figure shows the drying tests for each drying air

312 temperature. Drying times are very long for 100ºC and 125ºC regardless of the velocity,

313 between 7 and 23 hours. However, for temperatures greater than 125ºC, the drying

314 times are much shorter. The higher the drying temperatures, the lower the drying times.

315 However, for these three temperatures, 150ºC, 175ºC and 200ºC, the air velocity hardly

316 affects the drying process. Drying times for these temperatures ranged from 2 and 5

317 hours.

318

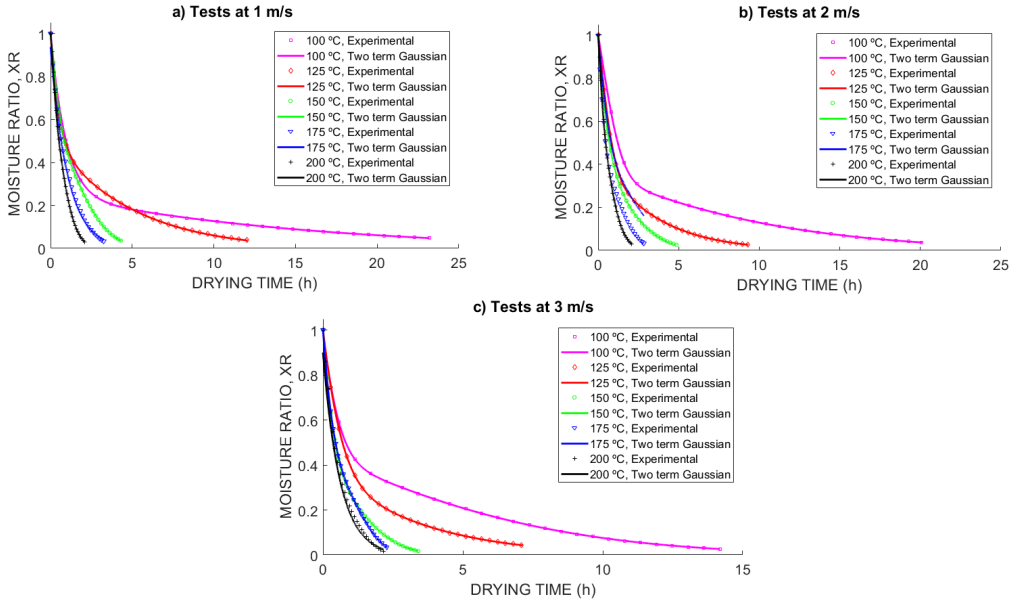

Figure 2: Drying curves during the drying process of mango stone at different drying air velocities: **a)** 1 m/s, **b)** 2 m/s and **c)** 3 m/s.

An interesting behavior is observed for experiments carried out at 100ºC and 125ºC for all air velocities. When the drying time was between two and three hours, a meaningful change of tendency was observed. The angle of the drying curve decreases considerably. This phenomenon occurs for moisture ratios between 0.2 and 0.4. This fact can be explained by taking into account that water elimination is easier on the external surface of the samples. The water contained in the fibres and pulp attached to the shell of the mango stone is evaporated between two and three hours. However, the water migration from the seed to the outside is very difficult, mainly due to the low permeability of the shell. This fact impacts the drying time making them much longer. This behaviour indicates that the main driving force in the drying process is temperature. It is essential to indicate that for these low temperatures, the drying air velocity plays a role very important in the mass convection in the external surface of the shell, decreasing the drying time (Huang et al., 2022). For example, drying test A, at 100ºC and 1 m/s, was approximately 23 hours while drying the test K, at 100ºC and 3

m/s, was 14 hours.

On the other hand, the samples experimented with darkening the external surface. Figure 3a-f shows the darkening of the sample for different drying times for the test N performed at 175ºC and 3 m/s. Darkening started in the slimmest sections where the moisture content decreased rapidly. Surfaces exposed to high drying air temperatures usually present risk of combustion. In this research, samples did not burn. However, in the drying experiments carried out at 200ºC, the release of volatile particles was observed when the moisture content was near the equilibrium moisture content. This behaviour has been seen during the drying of other biomass by-products such as spent coffee grounds (Gómez-de la Cruz, F. J., Palomar-Carnicero, Hernández-Escobedo and Cruz-Peragón, 2021), olive mill wastes (Arjona et al., 1999) and olive stone (Gómez-De La Cruz, F. J. et al., 2015a). On the other hand, a small decrease in the volume of the samples can be seen in the external pulp linked to the shell. In the final, the seed is totally crushed, however, the samples did not show shrinkage in all experiments. This behaviour has been appreciated in other tropical fruit seed as Hass avocado (Avhad and Marchetti, 2016).

Experimental data of drying curves have been fitted from the Two-term Gaussian model (Eq.4). Statistical parameters can be seen in table 3.

362 **Table 3.** Coefficient of determination and root mean square error for the Two-term Gaussian model
363 fit for each experiment.

TEST	R^2	RMSE
A	0.9985 ± 0.0001	0.014481 ± 3x 10^{-6}
B	0.9999 ± 0.0001	0.005255 ± 2x 10^{-6}
C	0.9999 ± 0.0001	0.005309 ± 3x 10^{-6}
D	0.9999 ± 0.0001	0.005891 ± 4x 10^{-6}
E	0.9996 ± 0.0001	0.010342 ± 3x 10^{-6}
F	0.9995 ± 0.0002	0.006079 ± 2x 10^{-6}
G	0.9993 ± 0.0002	0.008999 ± 4x 10^{-6}
H	1 ± 0.0001	0.002311 ± 1x 10^{-6}
I	0.9999 ± 0.0001	0.004311 ± 2x 10^{-6}
J	0.9998 ± 0.0001	0.007209 ± 2x 10^{-6}
K	0.9994 ± 0.0002	0.011491 ± 3x 10^{-6}
L	0.9998 ± 0.0001	0.004311 ± 2x 10^{-6}
M	0.9999 ± 0.0001	0.003675 ± 3x 10^{-6}
N	0.9999 ± 0.0001	0.003909 ± 3x 10^{-6}
O	0.9999 ± 0.0001	0.003494 ± 3x 10^{-6}

364

365

366

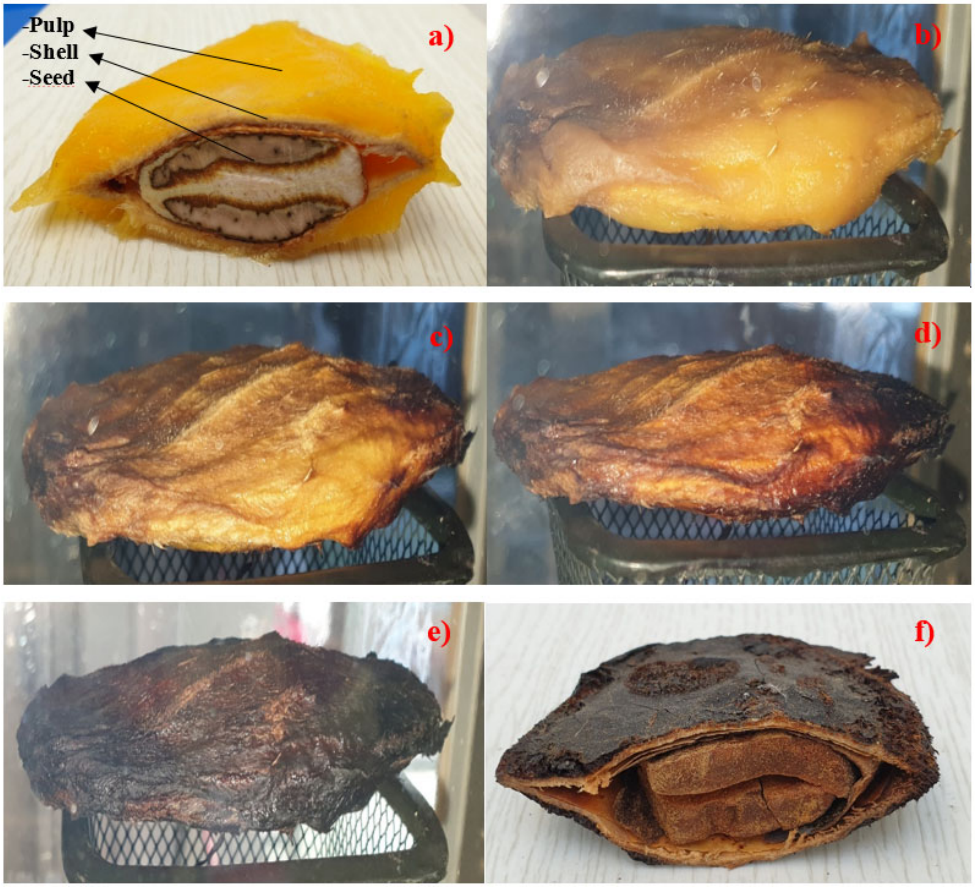

Figure 3: Moisture content and aspect evolution of the mango stone samples during the drying process for the test N: **a)** Initial moisture content and cross-section, **b)** 59% (wet basis), **c)** 46.02% (wet basis), **d)** 37.1% (wet basis), **e)** 8.6% (wet basis), **f)** equilibrium moisture content and cross-section.

3.2. Evaluation of the drying rate.

The drying rate has been obtained as a function of moisture ratio and temperature for each air velocity. To do this, first, the drying rate was calculated for each test from the derivate of the Two-term Gaussian model (Eq. (4)), since the drying rate from experimental data presented large fluctuations (Figure 4a). The model presented average R^2 and $RMSE$ values of 0.99968 and 0.006463, respectively. Figure 4b-d shows the polynomial surface that fits the experimental data with a fourth-degree in XR and fifth-degree in T. To perform the function, the linear least-squares fitting method was used with a coefficient of determination and a root mean square error of 0.9931 and $1.341 \cdot 10^{-}$

382 ^{5} (for 1 m/s), 0.9989 and $5.71 \cdot 10^{-6}$ (for 2 m/s) and 0.9976 and $1.07 \cdot 10^{-5}$ (for 3 m/s),

383 respectively.

384

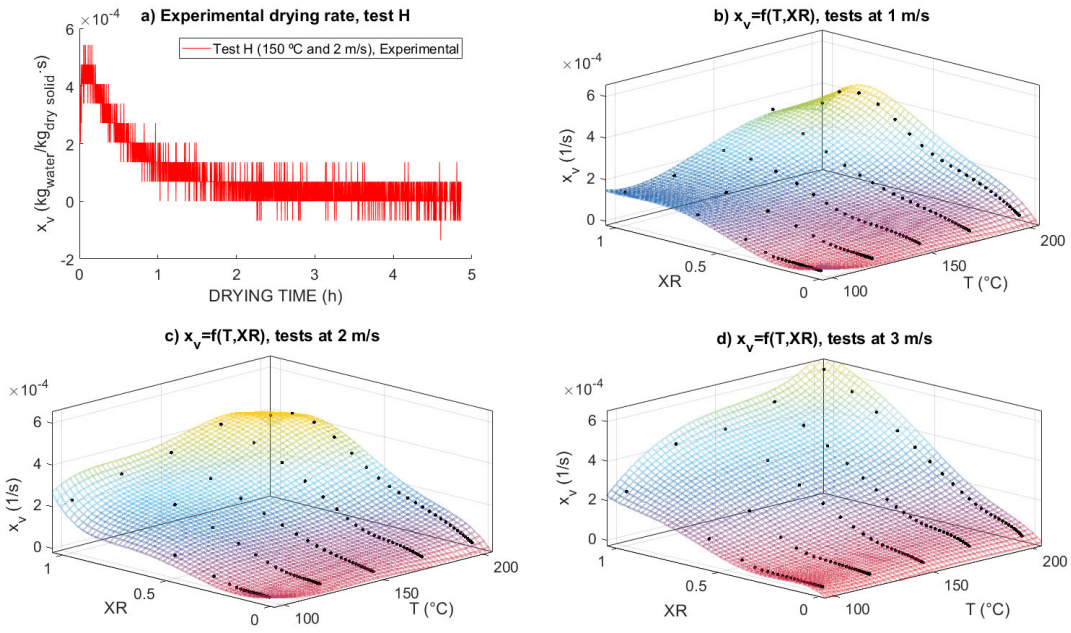

385

386 **Figure 4: a)** Fluctuations in the experimental drying rate calculation, **b)** drying rate at 1 m/s, **c)**
387 drying rate at 2 m/s and **d)** drying rate at 3 m/s.
388

389 Figure 4b-d depicts the different drying stages during the drying process of mango
390 stone: the warming-up period, the first falling rate period and the second falling rate
391 period (Chen, D. et al., 2012). In the first period, the maximum values of the drying rate
392 were found between $2 \cdot 10^{-4}$ and $4 \cdot 10^{-4}$ s^{-1} for tests performed at 1 m/s and 2 m/s at the
393 beginning of the process. For tests carried out at 3 m/s drying rates were found between
394 $4 \cdot 10^{-4}$ and $6 \cdot 10^{-4}$ s^{-1} at temperatures higher than 125 ºC. These results are higher than
395 those obtained by Wilkins et al., 2018 during the solar drying of mango waste at low
396 temperatures. In this stage, the sample surface, which is formed by mango pulp affixed
397 to the sell, is totally wet and the water evaporation is fast. Here, the drying air
398 temperatures above 100 ºC originate high vapour pressures. The warming-up period
399 tends to disappear as the air velocity increases regardless of the temperature.

400 The falling rate period occurs in practically all drying process, which is governed
401 by the convection and diffusion phenomenon (Richter Reis et al., 2017). The limit
402 between the first and second falling rate period can be perfectly seen for tests between
403 100ºC and 150ºC where the slope changes strongly due mainly to the barrier
404 phenomenon that presents the shell to eliminate the water contained in the seed, as was
405 commented in section 3.1. At these temperatures, in the second falling rate period the
406 drying rates decrease slightly up to the equilibrium content. In this stage, diffusion is the
407 predominant phenomenon where the external surface of the sample is totally dry and the
408 water migration is carried out from seed to surrounding air throughout the shell (Zhao et
409 al., 2021). As expected, the best range of temperature and velocity that minimizes the
410 drying time and increases the drying rates is found to be between 150 ºC and 200 ºC and
411 2 and 3 m/s, respectively.
412
413 3.3. Determination of effective diffusivity and activation energy.
414
415 Table 4 indicates the effective diffusivity values obtained for each test. The results
416 showed that this variable increases as the drying air temperature and velocity increase as
417 well. The experiments performed at the temperatures 150ºC, 175ºC and 200ºC presented
418 effective diffusivity values higher than those carried out at 100ºC and 125ºC. This fact
419 newly indicates the barrier effect that presents the shell of the mango stone sample at
420 low temperatures. In general, effective diffusivity is an overall parameter that includes
421 all complex phenomena during drying and plays a fundamental role in the design,
422 optimization, drying kinetics and mass transfer (Zheng et al., 2023). Figure 5 depicts
423 the tendency of effective diffusivity taking into account the drying air temperature and
424 velocity, but furthermore include other variables such as moisture content, thickness and

425 nature of the product. The results obtained ranged from $0.71 \cdot 10^{-9}$ to $13.6 \cdot 10^{-9}$ m^2/s.

426

427 **Table 4.** Effective diffusivity values and the coefficient of determination for each experiment.

TEST	D_{eff} x 10^9 (m^2/s)	R^2
A	0.71 ± 0.03	0.9530 ± 0.0022
B	2.66 ± 0.02	0.9765 ± 0.0013
C	5.40 ± 0.01	0.9905 ± 0.0004
D	7.69 ± 0.01	0.9960 ± 0.0009
E	13 ± 0.02	0.9649 ± 0.0018
F	1.01 ± 0.05	0.8739 ± 0.0065
G	2.74 ± 0.04	0.9391 ± 0.0052
H	5.38 ± 0.01	0.9969 ± 0.0003
I	8.53 ± 0.02	0.9889 ± 0.0012
J	13.2 ± 0.02	0.9824 ± 0.0022
K	1.65 ± 0.02	0.9837 ± 0.0018
L	2.95 ± 0.02	0.9826 ± 0.0015
M	5.98 ± 0.01	0.9919 ± 0.0008
N	9.75 ± 0.01	0.9895 ± 0.0018
O	13.6 ± 0.02	0.9814 ± 0.0022

428
429

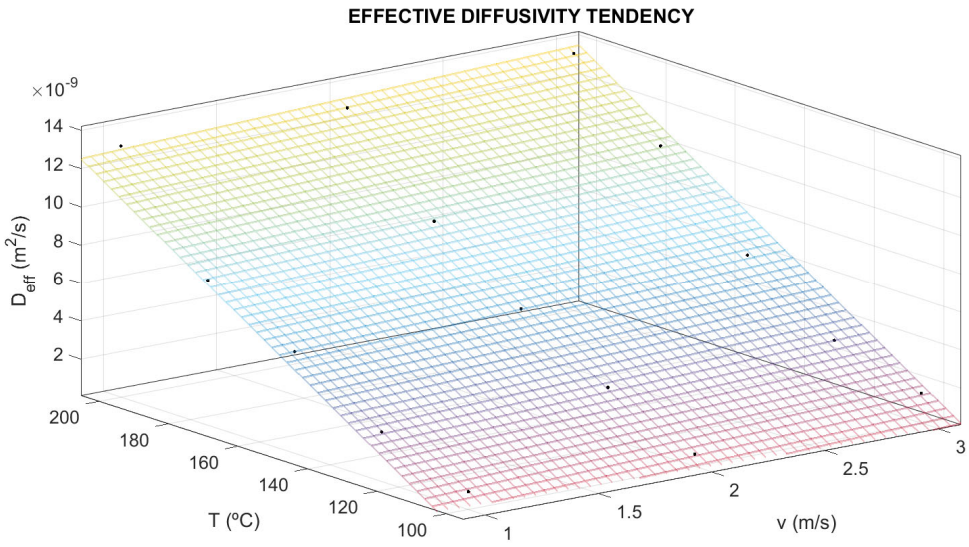

430

431 **Figure 5.** Effective diffusivity tendency considering the drying air temperature and velocity.

432

433 Activation energy is the variable that allows obtaining the power required for

434 moisture transmission during the drying, design and modelling mass transfer processes

435 (Mishra et al., 2021). It is a property characteristic of a substance and that depends on
436 its nature, geometry and drying conditions. These values were obtained for each drying
437 air temperature considering the five temperatures (figure 6). As expected, the results
438 indicate that the activation energy value is lower as the air velocity rises (table 5).
439 However, this value seems to be stabilizing at 3 m/s, suggesting that this variable does
440 not depend on the drying air velocity for higher values. This fact shows that fast water
441 diffusion in the sample depends strongly on the temperature and do not depend on the
442 air velocity for values higher than 2 m/s.
443

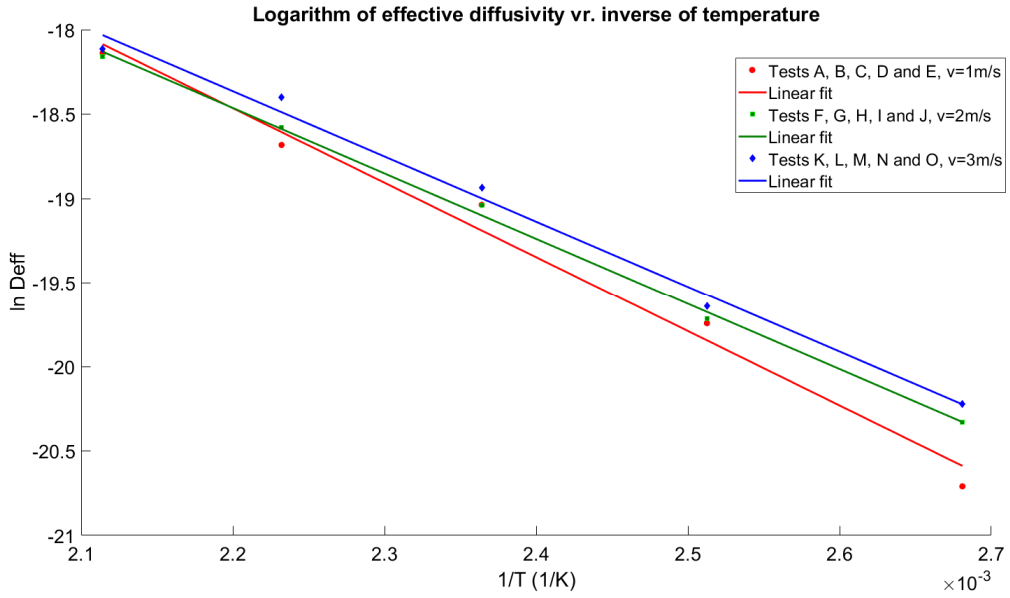

444

445 **Figure 6.** Arrhenius-type relationship between effective diffusivity logarithmic and the reciprocal of
446 absolute temperature for different drying air velocities.
447

448 **Table 5.** Activation energy, pre-exponential factor and coefficient of determination values for each
449 air velocity.

v (m/s)	E_a (kJ/mol)	D_0 (m^2/s)	R^2
1	36.7 ± 0.36	$1.581 \cdot 10^{-4} \pm 4x\ 10^{-3}$	0.9857 ± 0.0025
2	32.2 ± 0.15	$4.859 \cdot 10^{-5} \pm 2x\ 10^{-3}$	0.9955 ± 0.0011
3	32.1 ± 0.18	$5.524 \cdot 10^{-5} \pm 3x\ 10^{-3}$	0.9922 ± 0.0015

450

451

Effective moisture diffusivity and the activation energy values of mango stone are not found in the literature, but similar results were obtained for mango slices. Goyal et al., 2006 obtained in a convective dryer effective diffusivity values between $2.62 \cdot 10^{-10}$ and $4.39 \cdot 10^{-10}$ m^2/s at 55, 60 and 65 ºC air temperatures. Recently, Wang et al., 2018 studied the drying of mango in an indirect forced convection solar dryer obtaining values between $6.41 \cdot 10^{-11}$ and $1.18 \cdot 10^{-10}$ m^2/s, over the temperature range of 40–52 °C. Akoy, 2014 found activation energy during the drying of a mango slice (3 mm) at 0.5 m/s in a convective air oven of 37.99 kJ/mol. Kumar et al., 2022 obtained values of 24.11 kJ/mol, 25.82 kJ/mol and 26.32 kJ/mol for sample thicknesses of 2 mm, 4 mm and 6 mm, respectively, during foam-mat drying of mango in a convective dryer.

For other biomasses some different can be observer according to the drying conditions. Claudio et al., 2022 found effective moisture diffusivities values between $9 \cdot 10^{-11}$ and $7 \cdot 10^{-10}$ m^2/s and activation energy values between 38 and 58 kJ/mol for drying temperatures between 55 and 85ºC and drying air velocities between 2.5 and 4 m/s for acai residues. Agbede et al., 2020 studied the drying kinetics of green microalgae and the effective moisture values ranged between $4.64 \cdot 10^{-10}$ and $3.91 \cdot 10^{-9}$ m^2/s and an activation energy value of 28.7 kJ/mol for temperatures between 50 and 70 ºC and different sample thicknesses in a solar dryer.

4. Conclusion.

Mango stone, which represents 10% of the total fruit weight, was drying at different drying air temperatures and velocities. During drying, mango stone presented darkening of the external surface without shrinkage. Samples did not burn. At low temperatures (100ºC and 125ºC), drying times are very long, until 23 hours, mainly due to the barrier

effect that presents the mango stone shell. At these temperatures, mass convection is very important decreasing the drying time considerably as the air velocity is increased. At high temperatures (150ºC, 175ºC and 200ºC), drying times ranged between 2 and 5 hours. Drying rate and effective diffusivity verified the results obtained in the experiments where the higher values of drying rate and effective diffusivity were found for high temperatures and velocities. The activation energy value tended to be constant from 3 m/s. According to the results obtained in this work, it would be interesting to carry out new studies on the drying of crushed mango stones. The energy consumption in this mechanics process would be very low with respect to the thermal process, and the drying times would be considerably reduced.

Acknowledgments.

This work has been conducted with the financial support of the Spanish *"Consejería Andaluza de Innovación, Ciencia y Empresa"* through the research project AGR-6131 (*"Modelado y Control de secadero rotativo de orujo"*) as part of the research program *"Proyectos de Excelencia de la Junta de Andalucía 2010-2014"*. The authors gratefully acknowledge the financial support provided.

References.

Agbede, O.O., Oke, E.O., Akinfenwa, S.I., Wahab, K.T., Ogundipe, S., Aworanti, O.A., Arinkoola, A.O., Agarry, S.E., Ogunleye, O.O., Osuolale, F.N., Babatunde, K.A., 2020. Thin layer drying of green microalgae (Chlorella sp.) paste biomass: Drying

501 characteristics, energy requirement and mathematical modeling, Bioresour. Technol.
502 Rep. 11, 100467. doi: 10.1016/j.biteb.2020.100467.
503
504 Ajila CM, Bhat SG, Prasada Rao, U. J. S., 2007. Valuable components of raw and ripe
505 peels from two Indian mango varieties. Food Chem. 102:1006-11; doi:
506 10.1016/j.foodchem.2006.06.036.
507
508 Akoy EOM. Experimental characterization and modeling of thin-layer drying of mango
509 slices, 2014. Int Food Res J. 21:1911-7.
510
511 Arjona R, García A, Ollero P, 1999. Drying of alpeorujo, a waste product of the olive
512 oil mill industry. J Food Eng. 41:229-34. Doi: 10.1016/S0260-8774(99)00104-1
513
514 Avhad, M.R., Marchetti, J.M., 2016. Mathematical modelling of the drying kinetics of
515 Hass avocado seeds, Ind. Crops Prod. 91, 76-87. Doi: 10.1016/j.indcrop.2016.06.035
516
517 Chen, C., Venkitasamy, C., Zhang, W., Khir, R., Upadhyaya, S., Pan, Z., 2020.
518 Effective moisture diffusivity and drying simulation of walnuts under hot air, Int. J.
519 Heat Mass Transf. 150, 119283. doi: 10.1016/j.ijheatmasstransfer.2019.119283
520
521 Chen, D., Li, K., Zhu, X., 2012. Determination of effective moisture diffusivity and
522 activation energy for drying of powdered peanut shell under isothermal conditions,
523 BioResour. 7, 3670-3678.
524

525 Chupawa, P., Suksamran, W., Jaisut, D., Ronsse, F., Duangkhamchan, W., 2022.
526 Combined Heat and Mass Transfer Associated with Kinetics Models for Analyzing
527 Convective Stepwise Drying of Carrot Cubes, Foods. 11(24), 4045. doi:
528 10.3390/foods11244045
529
530 Claudio, C.C., Perazzini, M.B., Perazzini, H., 2022. Modeling and estimation of
531 moisture transport properties of drying of potential Amazon biomass for renewable
532 energy: Application of the two-compartment approach and diffusive models with
533 constant or moisture-dependent coefficient, Renew. Energy. 181, 304-316. doi:
534 10.1016/j.renene.2021.09.054
535
536 Crank J., (1975). The mathematics of diffusion. . Oxford, England: Clarendon Press.
537
538 Da Silva, A.C., Jorge, N., 2014. Bioactive compounds of the lipid fractions of agro-
539 industrial waste, Food Res. Int. 66, 493-500. Doi: 10.1016/j.foodres.2014.10.025
540
541 FAOSTAT, 2018. Food and Agriculture Data. Retrieved from:
542 http://www.fao.org/faostat/en/#home. Last consulted 02/01/2023.
543
544 Gómez-de la Cruz, F. J., Casanova-Peláez, P.J., Palomar-Carnicero, J.M., Cruz-
545 Peragón, F., 2014. Drying kinetics of olive stone: a valuable source of biomass obtained
546 in the olive oil extraction, Energy. 75, 146-152. Doi: 10.1016/j.energy.2014.06.085
547
548 Gómez-De La Cruz, F. J., Palomar-Carnicero, J.M., Casanova-Peláez, P.J., Cruz-
549 Peragón, F., 2015a. Experimental determination of effective moisture diffusivity during

the drying of clean olive stone: Dependence of temperature, moisture content and sample thickness, Fuel Process Technol. 137, 320-326. Doi: 10.1016/j.fuproc.2015.03.018

Gómez-de la Cruz, Francisco J, Casanova-Peláez, P.J., López-García, R., Cruz-Peragón, F., 2015b. Review of the Drying Kinetics of Olive Oil Mill Wastes: Biomass Recovery, BioResources. 10, 6055-6080. Doi: 10.15376/biores.10.3.Cruz

Gómez-de la Cruz, F. J., Casanova-Peláez, P.J., Palomar-Carnicero, J.M., Cruz-Peragón, F., 2017. Characterization and analysis of the drying real process in an industrial olive-oil mill waste rotary dryer: A case of study in Andalusia, Appl. Therm. Eng. 116, 1-10. Doi: 10.1016/j.applthermaleng.2017.01.050.

Gómez-de la Cruz, F. J., Palomar-Carnicero, J.M., Hernández-Escobedo, Q., Cruz-Peragón, F., 2020. Determination of the drying rate and effective diffusivity coefficients during convective drying of two-phase olive mill waste at rotary dryers drying conditions for their application, Renew. Energy. 153, 900-910. Doi: 10.1016/j.renene.2020.02.062

Gómez-de la Cruz, F. J., Palomar-Carnicero, J.M., Hernández-Escobedo, Q., Cruz-Peragón, F., 2021. Experimental studies on mass transfer during convective drying of spent coffee grounds generated in the soluble coffee industry, J Therm Anal Calor. 145, 97-107. Doi: 10.1007/s10973-020-09600-3

574 Goyal, R.K., Kingsly, A.R.P., Manikantan, M.R., Ilyas, S.M., 2006. Thin-layer Drying
575 Kinetics of Raw Mango Slices, Biosyst. Eng. 95, 43-49. Doi:
576 10.1016/j.biosystemseng.2006.05.001
577
578 Huang, X., Li, Y., Zhou, X., Wang, J., Zhang, Q., Yang, X., Zhu, L., Geng, Z., 2022.
579 Prediction of Apple Slices Drying Kinetic during Infrared-Assisted-Hot Air Drying by
580 Deep Neural Networks, Foods. 11(21), 3486. Doi: 10.3390/foods11213486
581
582 Ishaq, H., Dincer, I., 2020. A new energy system based on biomass gasification for
583 hydrogen and power production, Energy Rep. 6, 771-781. Doi:
584 10.1016/j.egyr.2020.02.019
585
586 Jha, A., Tripathy, P.P., 2021. Optimization of process parameters and numerical
587 modeling of heat and mass transfer during simulated solar drying of paddy, Comput.
588 Electron. Agric. 187, 106215. Doi: 10.1016/j.compag.2021.106215
589
590 Kaya, A., Aydın, O., Dincer, I., 2008. Experimental and numerical investigation of heat
591 and mass transfer during drying of Hayward kiwi fruits (Actinidia Deliciosa Planch), J.
592 Food Eng. 88(3), 323-330. Doi: 10.1016/j.jfoodeng.2008.02.017
593
594 Kumar, A., Kandasamy, P., Chakraborty, I., Hangshing, L., 2022. Analysis of energy
595 consumption, heat and mass transfer, drying kinetics and effective moisture diffusivity
596 during foam-mat drying of mango in a convective hot-air dryer, Biosyst. Eng. 219, 85-
597 102. doi: 10.1016/j.biosystemseng.2022.04.026
598

599 Leanpolchareanchai, J., Padois, K., Falson, F., Bavovada, R., Pithayanukul, P., 2014.
600 Microemulsion system for topical delivery of Thai mango seed kernel extract:
601 Development, physicochemical characterisation and ex vivo skin permeation studies,
602 Molecules. 19, 17107-17129. Doi: 10.3390/molecules191117107.
603
604 Maneepun, S., Yunchalad, M., 2004. Developing processed mango products for
605 international markets, Acta Hortic. 645, 13.
606
607 Manhongo, T.T., Chimphango, A., Thornley, P., Röder, M., 2021. Techno-economic
608 and environmental evaluation of integrated mango waste biorefineries. J. Clean. Prod.
609 325, 129335. Doi: 10.1016/j.jclepro.2021.129335
610
611 Mirabella, N., Castellani, V., Sala, S., 2014. Current options for the valorization of food
612 manufacturing waste: A review, J. Clean. Prod. 65, 28-41. Doi:
613 10.1016/j.jclepro.2013.10.051
614
615 Mishra, M., Kandasamy, P., Shukla, R.N., Kumar, A., 2021. Convective Hot-air Drying
616 of Green Mango: Influence of Hot Water Blanching and Chemical Pretreatments on
617 Drying Kinetics and Physicochemical Properties of Dried Product, Int. J. Fruit Sci. 21,
618 732-757. Doi: 10.1080/15538362.2021.1930626
619
620 Perazzini, H., Leonel, A., Perazzini, M.T.B., 2021. Energy of activation, instantaneous
621 energy consumption, and coupled heat and mass transfer modeling in drying of sorghum
622 grains, Biosyst. Eng. 210, 181-192. Doi: 10.1016/j.biosystemseng.2021.08.025
623

624 Perea-Moreno, A., Perea-Moreno, M., Dorado, M.P., Manzano-Agugliaro, F., 2018.
625 Mango stone properties as biofuel and its potential for reducing CO2 emissions, J.
626 Clean. Prod. 190, 53-62. Doi: 10.1016/j.jclepro.2018.04.147
627
628 Richter Reis, F., Ivahashi, M.M., Guéniat Rosa, A.H., 2017. Effect of Vacuum Drying
629 Temperature on Drying Kinetics, Effective Moisture Diffusivity and Quality of Peeled
630 Litchi (Litchi chinensis Sonn), J. Food Process Eng. 40, 12419. Doi:
631 10.1111/jfpe.12419
632
633 Saidur, R., Abdelaziz, E.A., Demirbas, A., Hossain, M.S., Mekhilef, S., 2011. A review
634 on biomass as a fuel for boilers, Renewable Sustainable Energy Rev. 15, 2262-2289.
635 Doi: 10.1016/j.rser.2011.02.015
636
637 Torres-León, C., Rojas, R., Contreras-Esquivel, J.C., Serna-Cock, L., Belmares-Cerda,
638 R.E., Aguilar, C.N., 2016. Mango seed: Functional and nutritional properties, Trends
639 Food Sci. Technol. 55, 109-117. Doi: 10.1016/j.tifs.2016.06.009
640
641 Ture, S.A., Chandramohan, V.P., 2021. Effect of radiation heat transfer in convective
642 drying of cranberry: Numerical solutions of one and two dimensional heat and mass
643 transfer and comparison of results, Therm. Sci. Eng. Prog. 22, 100837. Doi:
644 10.1016/j.tsep.2020.100837
645
646 Wang, W., Li, M., Hassanien, R.H.E., Wang, Y., Yang, L., 2018. Thermal performance
647 of indirect forced convection solar dryer and kinetics analysis of mango, Appl. Therm.
648 Eng. 134, 310-321. Doi: 10.1016/j.applthermaleng.2018.01.115

649

650 Wilkins, R., Brusey, J., Gaura, E., 2018. Modelling uncontrolled solar drying of mango
651 waste, J. Food Eng. 237, 44-51. Doi 10.1016/j.jfoodeng.2018.05.012

652

653 Zhao, F., Han, F., Zhang, S.-., Zhang, Z.-., 2021. Vacuum-Drying of the
654 LiNi1/3Co1/3Mn1/3O2 Cathode Material, ACS Sustainable Chem. Eng. 9, 639-647.
655 Doi: 10.1021/acssuschemeng.0c04083

656

657 Zheng, Z., Wei, S., Xie, W., Ren, L., Fan, B., Fu, H., Yang, D., 2023. Determination
658 and comparison of effective moisture diffusivity of carrot (core and cortex) during hot
659 air drying, J. Food Process Eng. 46, e14236. Doi: 10.1111/jfpe.14236